

Received August 20, 2018, accepted October 18, 2018, date of publication November 9, 2018,
date of current version December 7, 2018.

Digital Object Identifier 10.1109/ACCESS.2018.2879436

MOSAIC: Simultaneous Localization and Environment Mapping Using mmWave Without A-Priori Knowledge

ALI YASSIN^{ID1}, YOUSSEF NASSER¹, (Senior Member, IEEE),

AHMED Y. AL-DUBAI^{ID2}, (Senior Member, IEEE),

AND MARIETTE AWAD¹

¹Department of Electrical and Computer Engineering, Maroun Semaan Faculty of Engineering and Architecture, American University of Beirut, Beirut 00961, Lebanon

²School of Computing, Edinburgh Napier University, Edinburgh EH10 5DT, U.K.

Corresponding author: Ali Yassin (ahy04@mail.aub.edu)

ABSTRACT Simultaneous localization and environment mapping (SLAM) is the core to robotic mapping and navigation as it constructs simultaneously the unknown environment and localizes the agent within. However, in millimeter wave (mmWave) research, SLAM is still at its infancy. This paper consists a first of its kind in mapping an indoor environment based on the RSS, Time-Difference-of-Arrival, and Angle-of-Arrival measurements. We introduce MOSAIC as a new approach for SLAM in indoor environment by exploiting the map-based channel model. More precisely, we perform localization and environment inference through obstacle detection and dimensioning. The concept of virtual anchor nodes (VANs), known in literature as the mirrors of the real anchors with respect to the obstacles in the environment, is explored. Then, based on these VANs, the obstacles positions and dimensions are estimated by detecting the zone of paths obstruction, points of reflection, and obstacle vertices. Then, extended Kalman filter is adapted to the studied environment to improve the estimation of the points of reflection hence the mapping accuracy. Cramer–Rao lower bounds are also derived to find the optimal number of anchor nodes. Simulation results have shown high localization accuracy and obstacle detection using mmWave technology.

INDEX TERMS Millimeter wave, triangulation (TL), virtual anchor node (VAN), simultaneous localization and mapping, obstacle detection.

I. INTRODUCTION

Millimeter Wave (mmWave) wireless communication systems have recently gained great research interests due to their benefits in terms of spectrum, propagation characteristics, potential applications and services [1], [2]. The shortness of the coverage range of anchor nodes (ANs) operating at mmWave frequencies triggers the deployment of a capillary network of ANs in the buildings offering enhancements in terms of localization. Among the potential services offered by mmWave, localization and mapping appear as key factors in enabling new means and tools for communications systems [3], particularly indoor positioning systems (IPS).

Recently, IPS have been at the center of attention for researchers because of the vast technological enhancement in smart phones and tablets, and the evolving technology of Internet of Things (IoT) as a future service in 5G.

For instance, localization is critical for detecting products stored in a warehouse, medical equipment and personnel in a hospital, firemen in a building with fire, etc. With the evolution of mmWave communication systems, IPSs will exploit the infrastructure of future mmWave groundwork. In literature, there exist few researches on localization systems operating at mmWave frequencies. Most of the research work was focused on measuring the delay spread, Time-of-Arrival (TDoA), Time-Difference-of-Arrival (TDoA) and Angle-of-Arrival (AoA) methods [4], [5].

The channel characteristics at the mmWave frequencies differ from low frequencies range in many aspects; hence, the exploitation of these characteristics for localization and mapping should be totally revised and new approaches are to be proposed. At the same time, these properties open the door for additional applications such as mmWave based radar

systems. Indeed, researches have shown that the channel at mmWave behaves as quasi-optical channel in which the Line of Sight (LoS) ray is dominant. Moreover, it has been shown that the channel power exponentially decays in None-Line-of-Sight (NLoS) environment where a single-bounce is usually carrying most of the power. On the other hand, the characteristics of the channel at those frequencies showed that reflections don't generate significant amount of scattering [7], and that the transmitted beam will have the same directivity after reflections with slight scattering [8]. Hence, Snell's law holds in terms of the equality between the angles of departure and incidence upon reflection [9]. As a consequence, these propagation characteristics make the localization and mapping a very challenging task at mmWave. The appropriate localization procedures and mapping approaches should be then derived [10]–[12].

Originally, the concept of Simultaneous Localization and Mapping (SLAM) was achieved (in robotics) by moving a robot in an unknown environment to be recognized [13]. The process is based on steering a laser beam across a dense number of test directions. Then, the round-trip time (RTT) of the signal reflected by the obstacles is estimated in each direction. Hence, the distance to obstacles, inferred from the RTT, was used to build the indoor map. Accurate ranging and high angle resolution are the two main inputs for an accurate SLAM. Such aspects were usually achieved through laser technology. Despite the interest of the technology and the approach adopted therein, the system has to be as the technology has to be equipped with laser and mechanical steering devices; hence, it is complex and high-cost integration in mobile devices [14], [15]. At mmWave frequencies, very few works have dealt with SLAM approaches. We particularly mention the works of [13] and [16] where the authors proposed a radar-based system operating at mmWaves to overcome the shortcomings of laser. They provided high ranging accuracy using wideband signals and high directional antenna with mechanical steering. Technically, the reflected signal from the obstacle is scanned in front of the radar transceiver to estimate the distance from the obstacle. Thanks to the large system bandwidth and high temporal resolution of the paths, the proposed approaches therein have shown high accuracy. However, the system has to be in radar-like configuration, i.e. perpendicular to the obstacle, in order to have highly accurate mapping. We should mention that this radar-like system was possible in mmWaves as the latter promotes the implementation of massive antenna arrays at the ANs [17]–[20]. This is indeed possible due to the reduced size of antenna arrays. For instance, the works in [21]–[24] proposed new designs of personal radar with SLAM features using massive antenna arrays placed in a smart-phone or tablet. Likewise, Guidi *et al.* [25] adopted mmWave technology with multi-antenna radar system to scan the environment even if the smart-phone is kept in the user pocket. The concept of SLAM is expected to be widely spread in the future, especially in the domain of IoT [26].

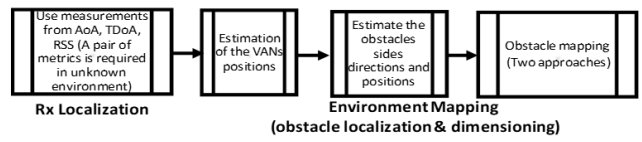


FIGURE 1. Steps needed in MOSAIC.

In this paper, our approach for SLAM in mmWave technologies is totally different. The proposed work does not impose any constraint on the receiver orientation and configuration; rather, it exploits the rays characteristics and the separation capabilities of these rays at the receiver to propose an innovative framework (called MOSAIC) for localization and mapping purposes. More precisely, the paper exploits one or more of the localization metrics, i.e. AoA, TDoA, and RSS, to achieve the obstacle detection, mapping and dimensioning. The latter are assumed to have different shapes and randomly distributed in the indoor environment. Throughout the paper, the system model is firstly derived for one AN and one receiver and then extended to multiple ANs. The number of ANs has been optimized through Cramer-Rao Lower Bounds (CRLB) derivations. The CRLBs outcomes are then used in the simulations to assess the proposed localization and mapping approaches.

Technically speaking, we will briefly introduce a first approach available in literature on the localization of a receiver (Rx) in a known environment using the concept of virtual anchor nodes (VANs). Then, as shown in Fig. 1, the concept of Rx localization is extended to unknown environment. In this case, MOSAIC proposes to exploit the information obtained by at least two channel metrics (TDoA, AoA, RSS) to estimate the Rx position. To implement a joint localization and mapping, MOSAIC is based on the estimation of the VANs positions, followed by the estimation of the obstacles sides directions and positions. It is followed by an adaptation of the Extended Kalman Filter (EKF) to have an improved mapping of the environment. Moreover, MOSAIC proposes two approaches for the obstacles dimensions (i.e. sides). This paper extends our previous work in [29] in which the room geometry has been identified using the AoA metric only. The contributions of this paper could be summarized as follows:

- Exploitation of the map-based mmWave channel characteristics to provide localization and mapping in indoor scenarios.
- Extension of our previous work in [29] based on AoA metrics to other metrics (RSS and TDoA): this extension is needed since in real scenarios these channel metrics are available and could be exploited to improve the localization and mapping accuracy
- Exploitation of the VANs principle widely used in literature to realize the obstacle positioning, dimensioning and mapping. In this paper, MOSAIC proposes two different approaches for mapping. The first one is based on

- estimating the cloud of reflection points (CoRP) belonging to the obstacle borders. The CoRP will be used to estimate the obstacles limits, positions and dimensions. The second is based on determining the obstacles vertices. EKF has been adapted to the obstacle mapping model, namely in improving the estimation of the CoRP.
- Derivation and exploitation of the CRLB to optimize the number of ANs needed to achieve a target accuracy.
 - Validation of proposed approaches through extensive simulation results. A professional mmWave ray tracing tool has been also used for the simulation results.

For the sake of clarification, the following notations will be adopted in the paper. A point in the environment starts with letter \mathbf{p} . For instance, \mathbf{pT} , \mathbf{pR} and \mathbf{pV} stand for the transmitter, receiver and VAN positions. The index k stands for time while i stands for the i^{th} received ray component (RRC) respectively. Also, the subscript notation (i, j) is used to indicate the difference in measurement between the element i and element j while the subscript m refers to an AN. Throughout the paper, the time index k is mentioned only when necessary for the sake of simplification of the model.

The rest of this paper is organized as follows. In Section 2, we develop the system model and the localization methodology of the receiver using mmWave. In Section 3, we introduce localization approaches in mmWave with an extension to unknown environment. In section 4, new approaches for context inference by estimating obstacles positions and dimensions are presented. In section 5, we adapt the EKF model to improve the estimation of the CoRPs when the receiver is moving in the studied environment. In Section 6, the effect of the number of ANs is discussed using the CRLB. Then, the simulation results for an indoor environment are provided in section 7, while conclusions are drawn in Section 8.

II. MOSAIC: SYSTEM MODEL AND ENVIRONMENT

A. SYSTEM ENVIRONMENT

We consider in this paper a 2D indoor environment consisting of a room bounded by 4 walls for the sake of simplicity. The extension to 3D environment is left for further work. The room geometry is assumed to be known with single transmitter and single receiver. This assumption does not change any step in the proposed approaches neither in the conclusions but makes the model simpler to argue. The room boundaries and radio-reflective obstacles in the reflective objects are grouped in a set O . Obstacles are described as two-dimensional flat polygonal faces with sharp vertices and straight edges. Each oriented obstacle S is denoted by its perpendicular line, described by:

$$y = yp + \alpha \cdot (x - xp) \quad (1)$$

where $\mathbf{p} = (xp, yp)$ is a point of intersection between the obstacle and its perpendicular and α is the slope of the line orthogonal to the obstacle S . By assumption, a single mmWave transmitter (Tx) is deployed in the room at a location \mathbf{pT} . Additionally, the transmitter is assumed to broadcast its position to the node(s) targeted for localization.

Throughout the paper, AoA will be the main metric for localization and mapping. It is very robust against power loss and absorption at mmWave [27]. The AoA spectrum has been widely used in literature [4], [5]. It gives the power received at each angle of arrival hence it is usually modeled as a $2 \times L$ matrix, $\mathbf{SP}(\theta)$, that records the amplitude of each RRC as a function of the azimuth θ at a given location \mathbf{p} , where L is the number of RRCs. Each RRC can be either due to a LoS link between the transmitter and the receiver or due to NLoS link caused by reflections of one or more surfaces in the obstacle set O . Localization in this case is achieved by observing NLoS paths as virtual LoS rays coming through virtual LoS links from VANs. A sorting in decreasing order of $\mathbf{SP}(\theta)$ according to the first row, i.e. to ray power, allows to characterize the received signal in which the first column has the highest power. In practice, if the receiver and transmitter are in LoS, this column represents θ_0 , the AoA of the LoS ray, and its corresponding power. The columns $2 : L$ represent the NLoS paths.

B. VIRTUAL ANCHORS

The concept of VAN in mmWaves has been introduced in literature. As shown in Fig. 2, it is based on the fact that each NLoS ray is emitted from a virtual anchor node placed at the mirror position of the transmitter with respect to the reflector. In LoS conditions, we might have $(L - 1)$ RRCs that correspond to NLoS paths. The locations of the VANs are determined by mirroring the transmitter \mathbf{pT} with respect to the surfaces in the obstacle set O since it is the source of signal reflections. We denote $V = \{pV_0, pV_1, \dots\}$ to be the set of the positions of all possible VANs, and we denote $\bar{V} = \{V_0, V_1, \dots\}$ to be a partition of V as follows. We let $V_0 = \mathbf{pT}$, and each set $V_i, i = 1, 2, \dots$ represents all VANs that have been mirrored i times due to reflections caused by any surface in the obstacle set O [28]. Actually, there is no limit on the number of reflections of the signal transmitted by \mathbf{pT} . However, a mmWave signal fades quickly during its propagation as it reflects off the surfaces. So, we limited the set \bar{V} by assuming a maximum reflection order $\mu = 1$ in this paper.¹ Hence, the set of all VANs will be represented as $V_\mu = \bigcup_{i=0}^{\mu} V_i$. As shown in Fig. 2, the anchors \mathbf{pV}_i and \mathbf{pV}_j represent first and second order of reflection respectively; hence, $\mathbf{pV}_i \in V_1$ and $\mathbf{pV}_j \in V_2$. Nevertheless, we limited μ for single reflection.

III. LOCALIZATION USING mmWAVES

In this section, we consider a harsh environment with one Tx and one Rx only. We tackle the problem of localization in mmWave while mainly based on AoA measurements due its robustness against power loss in mmWave [27]. Other measurement metrics such as TDoA and RSS are needed if the environment map is unknown.

¹The number of reflections at mmWave is usually limited to 2 as the power is almost negligible afterwards. In this paper, $\mu = 2$ is left for further studies

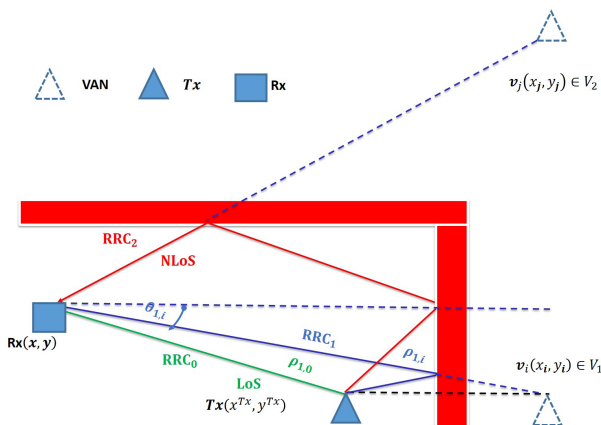


FIGURE 2. VANs related to first (RRC_1) and second order (RRC_2) of reflections.

A. THE TRIANGULATION (TL) ALGORITHM IN KNOWN ENVIRONMENT: AN AoA BASED APPROACH

This algorithm is based on estimating the location of a receiver at position \mathbf{pR} using a set of triangulation steps followed by a verification of the estimated positions [28], [29]. In this section and for the sake of clarification, we assume that the location orientation and dimensions of the obstacle are known at the receiver.

The TL provides good accuracy with low complexity versus the conventional maximum likelihood (ML) algorithm.² TL steps are based on forming a triangle between the unknown receiver and each VAN. As shown in Figure 2, the following relations are constructed using trigonometric relations in the right triangle formed between the receiver \mathbf{pR}_k at time k and VAN \mathbf{pV}_i as follows:

$$xV_i - xR_k = \rho_{k,i} \cdot \cos \theta_{k,i} \quad (2)$$

$$yV_i - yR_k = \rho_{k,i} \cdot \sin \theta_{k,i} \quad (3)$$

where $\mathbf{pV}_i = (xV_i, yV_i)$ and $\mathbf{pR}_k = (xR_k, yR_k)$ are the VANs and the unknown receiver respectively. $\theta_{k,i}$ and $\rho_{k,i}$ are the AoA and the distance of the RRC "transmitted virtually" from the VAN \mathbf{pV}_i to the receiver at position \mathbf{pR}_k , respectively. In this section, we aim at estimating the position of the receiver, i.e. xR_k and yR_k in (2) and (3). Hence, using $\theta_{k,i}$ and \mathbf{pV}_i (assumed known in this section), the problem turns out to find $\rho_{k,i}$. The latter could be easily estimated by simply differentiating between the signal originated from different VANs. Hence, for each pair of VANs \mathbf{pV}_i and \mathbf{pV}_j , the following equation holds:

$$\mathbf{V} = \Gamma \cdot \Xi \quad (4)$$

where \mathbf{V} , Γ , and Ξ are defined as follows:

$$\mathbf{V} = \begin{bmatrix} xV_i - xV_j \\ yV_i - yV_j \end{bmatrix}$$

$$\Gamma = \begin{bmatrix} \cos \theta_{k,i} - \cos \theta_{k,j} \\ \sin \theta_{k,i} - \sin \theta_{k,j} \end{bmatrix}$$

²For a fair comparison, ML results will be provided in the simulations results section.

$$\Xi = \begin{bmatrix} \rho_{k,i} \\ \rho_{k,j} \end{bmatrix}$$

Solving (4), we obtain:

$$\Xi = \Gamma^{-1} \cdot \mathbf{V}_{i,j} \quad (5)$$

Knowing Ξ , the estimation of the position \mathbf{pR}_k of the receiver can be done by inserting $\rho_{k,i}$ in (2) and (3). The TL steps are repeated I times, that is the total number of all possible pairs of $(\mathbf{pV}_i, \mathbf{pV}_j)$, $i \neq j$ in the set V_1 .

B. Rx LOCALIZATION IN UNKNOWN ENVIRONMENT

When the environment is unknown (i.e. there is no information on the obstacles in the room), the first step of the TL approach could not be applied as the VANs positions are unknown. To solve this problem, additional localization metrics such as TDoA and RSS³ are considered. Indeed, if for instance both AoA and TDoA measurements are available, the rays of both metrics are sorted in a decreasing order in terms of power. The first ray will be denoted as the LoS and the rest are the NLoS rays. The receiver position will be then deduced as the intersection point which verifies both the AoA and TDoA based distance equations. The algorithm for Rx localization is defined as follows.

- Find the distance between \mathbf{pT} and \mathbf{pR}_k using TDoA measurements of the first path. Theoretically, the distance of travel for the first ray is calculated from the TDoA as follows:

$$\rho_{k,0} = c \cdot t_{k,0} \quad (6)$$

where c is the speed of light, $\rho_{k,0}$ is the distance traveled by the first ray (LoS ray) and $t_{k,0}$ is the TDoA of the first ray, assumed to be in LoS.

- Find $\theta'_{k,0}$, the triangulated angle of $\theta_{k,0}$ i.e. the AoA of the first ray (LoS ray), as follows:

$$\begin{cases} \theta'_{k,0} = \pi/2 - \theta_{k,0}, & 0 \leq \theta_{k,0} \leq \pi/2 \\ \theta'_{k,0} = \theta_{k,0} - \pi/2, & \pi/2 \leq \theta_{k,0} \leq \pi \\ \theta'_{k,0} = 3\pi/2 - \theta_{k,0}, & \pi \leq \theta_{k,0} \leq 3\pi/2 \\ \theta'_{k,0} = \theta_{k,0} - 3\pi/2, & 3\pi/2 \leq \theta_{k,0} \leq 2\pi \end{cases} \quad (7)$$

- Using (6) and (7), estimate the position of the receiver as follows:

$$\mathbf{pR}_k = \mathbf{pT} + \rho_{k,0} \cdot \Omega \cdot \begin{bmatrix} \sin \theta'_{k,0} \\ \cos \theta'_{k,0} \end{bmatrix} \quad (8)$$

where $\mathbf{pR}_k = [xR_k \ yR_k]^T$, $\mathbf{pT} = [xT \ yT]^T$ and Ω is defined as follows:

$$\begin{cases} \Omega = \begin{bmatrix} -1 & -1 \end{bmatrix}^T, & 0 \leq \theta_{k,0} \leq \pi/2 \\ \Omega = \begin{bmatrix} 1 & -1 \end{bmatrix}^T, & \pi/2 \leq \theta_{k,0} \leq \pi \\ \Omega = \begin{bmatrix} 1 & 1 \end{bmatrix}^T, & \pi \leq \theta_{k,0} \leq 3\pi/2 \\ \Omega = \begin{bmatrix} -1 & 1 \end{bmatrix}^T, & 3\pi/2 \leq \theta_{k,0} \leq 2\pi \end{cases} \quad (9)$$

³These measurements are primordial for channel estimation at mmWaves

It is very clear from these derivations that localization in mmWave can be easily done with or without environment knowledge as long as there is sufficient measurements. Moreover, it is straightforward to mention that the availability of the LoS components highly improves the accuracy of the localization approaches. In case the LoS ray is not available, the estimation of the Rx position will be biased. However, as shown in [30], the estimation error could be very small if appropriate algorithms are implemented. In this paper, we are not proposing any approach for separation between LoS and NLoS yet the approach in [30] is easily adopted.

IV. CONTEXT INFERENCE AND OBSTACLE MAPPING IN MOSAIC

The main target of this section is to estimate obstacles locations and their dimensions using the received signal at Rx. MOSAIC implements obstacle detection in two steps: (1) estimating the position of the VANs using TL (i.e. using AoA), RSS and TDoA; (2) estimating the obstacle direction, points of reflection and obstacle dimensions.⁴ Tracking and filtering through EKF is then used to enhance the mapping accuracy.

A. ESTIMATION OF VANs POSITIONS

Here, three different algorithms are proposed depending on the available measurement metrics. The first algorithm is based on the TL discussed earlier, the second one is based on the TDoA while the third is based on RSS.

1) ALGORITHM 1- TL FOR ESTIMATING VANs

As stated above, the first step for mapping consists in estimating the positions of the VANs. However, these depend on the obstacles whose positions and dimensions are assumed unknown. Mathematically speaking, this requires estimating the different parameters $(x_{Vi}, y_{Vi}, \rho_{k,i})$ which represent the coordinates of the VANs and their distances with respect to the receiver.

The scenario is developed under harsh conditions, i.e. one transmitter and one receiver are only available for both localization and context inference. Hence, to deal with these conditions, we propose to move the receiver step-by-step while collecting new estimation. Technically, the estimation of $(x_{Vi}, y_{Vi}, \rho_{k,i})$ depends on the relative position of the receiver with respect to the VANs, as shown in Fig. 3. For instance, assuming that the AoA for the LoS path between the transmitter and receiver and the AoA for the NLoS path (LoS virtually) between the transmitter and receiver (VAN and receiver) fall in the first quadrant, the system of equations describing the relation between the different parameters in $(x_{Vi}, y_{Vi}, \rho_{k,i})$ defined in (2) and (3) is as

⁴All the calculations hereafter are presented in ideal conditions, i.e. without measurements errors, for the sake of simplification. However, in simulations, a bias due to measurements errors is added to different models

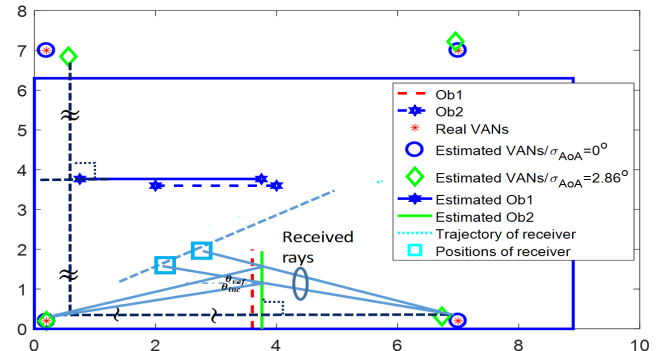


FIGURE 3. Estimated VANs by moving the receiver from \mathbf{pR}_k to \mathbf{pR}_{k+1} .

follows:

$$\begin{cases} x_{Vi} - xR_k = \rho_{k,i} \cdot \cos \theta_{k,i} \\ xR_k - xT = \rho_{k,0} \cdot \sin \theta_{k,0} \end{cases} \quad (10)$$

$$\begin{cases} y_{Vi} - yR_k = \rho_{k,i} \cdot \sin \theta_{k,i} \\ yR_k - yT = \rho_{k,0} \cdot \cos \theta_{k,0} \end{cases} \quad (11)$$

where $\rho_{k,0}$ is the distance between the receiver position at time k and the transmitter, $\theta_{k,0}$ is the AoA for the LoS link between the transmitter and the receiver, $\rho_{k,i}$ is the distance between the VAN to be localized and the original receiver position and $\theta_{k,i}$ is the AoA for the NLoS link corresponding to \mathbf{pV}_i . By solving the above two systems of equations, we obtain:

$$\begin{cases} x_{Vi} - xT = \rho_{k,0} \cdot \sin \theta_{k,0} + \rho_{k,i} \cdot \cos \theta_{k,i} \\ y_{Vi} - yT = \rho_{k,0} \cdot \cos \theta_{k,0} + \rho_{k,i} \cdot \sin \theta_{k,i} \end{cases} \quad (12)$$

The receiver now is moved to a new position \mathbf{pR}_{k+1} as shown in Fig. 3 so that we can solve the new system of equations where the unknown variables become the positions of the VANs.

The latter defines the relation between the parameters in $(x_{Vi}, y_{Vi}, \rho_{k,i})$ corresponding to the new receiver position is:

$$\begin{cases} x_{Vi} - xT = \rho_{k+1,0} \cdot \sin \theta_{k+1,0} + \rho_{k+1,i} \cdot \cos \theta_{k+1,i} \\ y_{Vi} - yT = \rho_{k+1,0} \cdot \cos \theta_{k+1,0} + \rho_{k+1,i} \cdot \sin \theta_{k+1,i} \end{cases} \quad (13)$$

where $\rho_{k+1,i}$ and $\theta_{k+1,i}$ are the distance and the AoA, respectively, corresponding to the link between the VAN \mathbf{pV}_i and the new receiver position \mathbf{pR}_{k+1} . Then, the estimation of the VANs is done by combining the two systems of equations in (12) and (13). This leads to the following:

$$\begin{bmatrix} \cos \theta_{k,i} & -\cos \theta_{k+1,i} \\ \sin \theta_{k,i} & -\sin \theta_{k+1,i} \end{bmatrix} \begin{bmatrix} \rho_{k,i} \\ \rho_{k+1,i} \end{bmatrix} = \begin{bmatrix} -\sin \theta_{k,0} & \sin \theta_{k+1,0} \\ -\cos \theta_{k,0} & \cos \theta_{k+1,0} \end{bmatrix} \begin{bmatrix} \rho_{k,0} \\ \rho_{k+1,0} \end{bmatrix} \quad (14)$$

The two unknowns, $\rho_{k,i}$ and $\rho_{k+1,i}$, are calculated as follows:

$$\begin{bmatrix} \rho_{k,i} \\ \rho_{k+1,i} \end{bmatrix} = \Sigma^{-1} \begin{bmatrix} -\sin \theta_{k,0} & \sin \theta_{k+1,0} \\ -\cos \theta_{k,0} & \cos \theta_{k+1,0} \end{bmatrix} \begin{bmatrix} \rho_{k,0} \\ \rho_{k+1,0} \end{bmatrix} \quad (15)$$

where $\Sigma = \begin{bmatrix} \cos \theta_{k,i} & -\cos \theta_{k+1,i} \\ \sin \theta_{k,i} & -\sin \theta_{k+1,i} \end{bmatrix}$.

$\rho_{k,i}$ and $\rho_{k+1,i}$ are then replaced in (12) or (13) to estimate xV_i and yV_i . Knowing that RRCs come from the transmitter via a LoS link and from VANs via NLoS links, this process is iterated over all entries of the AoA power spectrum $SP_p(\theta)$, a $(2 \times L)$ matrix, to estimate the positions of all VANs. The calculations are repeated at every receiver position.

2) ALGORITHM 2- TDoA FOR ESTIMATING VANs

TDoA can be also used for the estimation of the VANs. The distances between the receiver and the VAN \mathbf{pV}_i in absence of noise is represented as follows:

$$\rho_{(0,i)} = c \cdot t_{(0,i)} = \rho_i - \rho_0, \quad i = 1, \dots, L-1 \quad (16)$$

where $t_{(0,i)}$ is the TDoA of the received signal at the pair of the VAN \mathbf{pV}_i and the transmitter respectively, and c is the speed of the signal propagation. As shown in (16), the estimated TDoAs are converted to range difference of arrival (RDoA) measurements creating a set of nonlinear equations describing the hyperbolic range difference. The receiver position can be estimated from the intersection of the resultant hyperboloids. In realistic scenarios, RDoA measurements $\tilde{\rho}_{(0,i)}$ are obtained with noise as modeled in the following equation:

$$\tilde{\rho}_{(0,i)} = \rho_{(0,i)} + \epsilon_{(0,i)} = \rho_i - \rho_0 + \epsilon_{(0,i)}, \quad i = 1, \dots, L-1 \quad (17)$$

where $\epsilon_{(0,i)}$ is the zero mean Gaussian random noise vector of the RDoA measurement. Equation (17) can be written as $\tilde{\rho}_{(0,i)} + \rho_0 = \rho_i + \epsilon_{(0,i)}$. Hence, squaring and substituting with (58), we obtain:

$$\begin{aligned} & xR(xV_i - xT) + yR(yV_i - yT) + \rho_0\tilde{\rho}_{(0,i)} \\ &= \frac{1}{2} \left[(xV_i^2 - xT^2) + (yV_i^2 - yT^2) - \tilde{\rho}_{(0,i)}^2 \right] \\ &+ \frac{1}{2} \epsilon_{(0,i)}^2 + \rho_i\epsilon_{(0,i)} \end{aligned} \quad (18)$$

Hence, the model is given by:

$$\mathbf{G} \cdot \mathbf{pR} = \mathbf{H} \quad (19)$$

where \mathbf{G} , and \mathbf{H} are defined as follows:

$$\begin{aligned} \mathbf{G} &= \begin{bmatrix} x_1 - xT & y_1 - yT \\ \vdots & \vdots \\ x_{L-1} - xT & y_{L-1} - yT \end{bmatrix} \\ \mathbf{H} &= \begin{bmatrix} \frac{1}{2} (q_{(0,1)} - \tilde{\rho}_{(0,1)}^2) - \rho_0\tilde{\rho}_{(0,1)} \\ \vdots \\ \frac{1}{2} (q_{(0,L-1)} - \tilde{\rho}_{(0,L-1)}^2) - \rho_0\tilde{\rho}_{(0,L-1)} \end{bmatrix} \end{aligned}$$

where $q_{(0,i)} = \mathbf{pV}_i^T \mathbf{pV}_i - \mathbf{pT}^T \mathbf{pT}$. Three TDoA measurements are observed at three different positions of the receiver \mathbf{pR}_k , \mathbf{pR}_{k+1} and \mathbf{pR}_{k+2} respectively. The following system of equations is constructed based on the difference between the measurements taken at \mathbf{pR}_k and \mathbf{pR}_{k+1} and those taken at \mathbf{pR}_k and \mathbf{pR}_{k+2} , respectively (20) and (21), as shown at the bottom of the next page:

Equations (20) and (21) can be written in matrix notations as:

$$\mathbf{G} \cdot \mathbf{pR}_d = \mathbf{H}_d \quad (22)$$

where \mathbf{pR}_d and \mathbf{H}_d are defined as follows:

$$\mathbf{pR}_d = [\mathbf{pR}_k - \mathbf{pR}_{k+1} \quad \mathbf{pR}_k - \mathbf{pR}_{k+2}] \quad (23)$$

$$\mathbf{H}_d = [\mathbf{H}_k - \mathbf{H}_{k+1} \quad \mathbf{H}_k - \mathbf{H}_{k+2}] \quad (24)$$

The Least Square (LS) solution of \mathbf{G} yields:

$$\hat{\mathbf{G}} = \mathbf{H}_d \cdot \mathbf{pR}_d^{-1} \quad (25)$$

As a result, the positions of the VANs are estimated as follows:

$$\begin{bmatrix} x_1 & y_1 \\ \vdots & \vdots \\ x_{L-1} & y_{L-1} \end{bmatrix} = \hat{\mathbf{G}} + \begin{bmatrix} xT & yT \\ \vdots & \vdots \\ xT & yT \end{bmatrix} \quad (26)$$

3) ALGORITHM 3- RSS FOR ESTIMATING VANs

See Appendix A.

It is worth mentioning that all these solutions could be easily updated to Weighted LS (WLS) or other estimators. Therein, we restrict ourself to the WLS solution for the RSS given in Appendix due to lack of space.

B. OBSTACLE DETECTION

After the estimation of the VANs, the target is to detect the obstacles in the room. Referring to Fig. 3, obstacle detection is achieved using either RSS and AoA or TDoA and AoA. The obstacle detection is done by the following steps at each Rx position k :

- The VANs positions are firstly estimated as detailed in the previous section.
- Since the VANs are the mirrors of the transmitter with respect to all surfaces of the obstacles in the room, the obstacles are then the perpendicular to the line connecting the transmitter to each estimated VAN respectively. The perpendicular line passes through the midpoint of the segment $[\mathbf{pV}_i \mathbf{pT}]$. The latter is calculated as follows:

$$\mathbf{pM}_i = \frac{\mathbf{pT} + \mathbf{pV}_i}{2} \quad (27)$$

where $\mathbf{pM}_i = (xM_i, yM_i)$. Then, the normal to the point of reflection (PoR) \mathbf{pS}_i corresponding to VAN \mathbf{pV}_i is calculated as follows:

$$\mathbf{n}_i = \mathbf{pT} - \mathbf{pV}_i \quad (28)$$

where $\mathbf{n}_i = (xn_i, yn_i)$.

- Equation (1) is used to write the obstacle surface, where α and $\mathbf{pM}_i = (xM_i, yM_i)$ are the slope and midpoint of segment $[\mathbf{pV}_i \mathbf{pT}]$, respectively. Fig. 3 shows the estimated obstacles by firstly estimating its location (the midpoint between Tx and VAN) and direction.
- Using the AoA and the estimated positions of the receiver, VAN and obstacle, the point of reflection at the

obstacle can be easily deduced. It is simply the point of intersection between the line $[\mathbf{pV}_i, \mathbf{pR}]$ and the obstacle line. Then, the vector crossing the PoR $\mathbf{S}_{k,i}$ from the receiver to the transmitter is represented as follows:

$$\mathbf{w}_i = \mathbf{pV}_i - \mathbf{pR} \quad (29)$$

where $\mathbf{w}_i = (x_{Wi}, y_{Wi})$. Then, we solve for the points of intersection between VANs and the receiver to estimate the PoRs as follows:

$$\mathbf{pS}_i = \mathbf{pR}$$

$$+ \left(\text{inv}(\text{diag}(\mathbf{n}_i \cdot \mathbf{w}_i)) \cdot ((\mathbf{pM}_i - \mathbf{pR}) \cdot \mathbf{n}_i)^T \right)^T \cdot \mathbf{w}_i. \quad (30)$$

- At each receiver measurement, this procedure is iterated over all pairs of $(\mathbf{pV}_i, \mathbf{pT}), i = 1, 2, \dots, L$, where L is the number of VANs. At each iteration, an estimated point of reflection belonging to the obstacle side is created. Using all these measurements, a cloud (set) of reflection points is generated.
- Using the CoRP, an interpolation between these points is applied. It is followed by a simple smoothing operation.

In summary, obstacle surfaces are detected and estimated using a set of connected reflection points. Using the concept of mirroring, we iterate over all pairs of $(\mathbf{pV}_i, \mathbf{pT})$ at each Rx position to detect an obstacle surface. Then, the problem turns down to estimate the obstacle limits.

C. OBSTACLE DIMENSIONING: FINDING THE OBSTACLE LIMITS

After detecting the direction of the obstacles in the room and the corresponding CoRP, the boundaries of the obstacle are left to be set. Here two approaches are proposed (jointly or separately):

Approach 1: Estimate the vertices by power measurements As shown in Fig. 4, a point of reflection is obtained at the obstacle if the receiver moves within the region of all possible reflections determined by the obstacle limits, the position of the transmitter, and the related VAN. Hence, the AoA/TDoA/RSS spectrum generated at all receiver positions will dramatically change when the receiver leaves the region of reflection. Indeed, mmWave signals suffer from absorption loss by each obstacle. Hence, a change in the

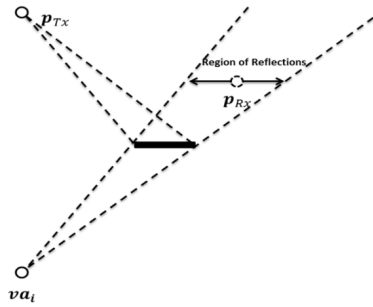


FIGURE 4. Region of possible reflections.

reflection environment will change when Rx changes from a region of reflection to another. Without loss of generality, when the receiver moves to the right or to the left outside the region of reflection shown in Fig. 4, the power of the received signal at the corresponding AoA will dramatically change raising the existence of the object limit. So the latter could be estimated by a simple border detection through power measurements, i.e separating the power of an obstacle ray from noise or walls rays. In this paper, the detection is based on a simple energy detector algorithm whose threshold is set to maximize the probability of detection.

Approach 2: Estimate the vertices as intersections of the obstacle sides: This approach could be applied if the obstacle is of 2D shape (not 1D). As shown in the previous section, each side of the obstacle is firstly determined via its direction and the CoRP. Hence, the limits (i.e. the vertices) of the obstacles are simply determined by the intersections of these sides.

To show the effectiveness of the proposed approaches, a simulation is executed in an indoor environment with a rectangular obstacle, a moving receiver across several positions and 4 transmitters as shown in Fig. 5. In this figure, it is very clear that the estimated points of reflection reproduce well the obstacle shape.

D. CLUSTERING THE CLOUD OF VERTICES POINTS

Each measurement at each Rx position provides an estimation of the point of reflection first and then, through obstacle limits calculations, provides an estimation of the vertices constituting the obstacle. However, as these measurements

$$\mathbf{G}(\mathbf{pR}_k - \mathbf{pR}_{k+1}) = \mathbf{H}_k - \mathbf{H}_{k+1} = \begin{bmatrix} \frac{1}{2} (\tilde{\rho}_{k+1,(0,1)}^2 - \tilde{\rho}_{k,(0,1)}^2) + \rho_{k+1,0}\tilde{\rho}_{k+1,(0,1)} - \rho_{k,0}\tilde{\rho}_{k,(0,1)} \\ \vdots \\ \frac{1}{2} (\tilde{\rho}_{k+1,(0,L-1)}^2 - \tilde{\rho}_{k,(0,L-1)}^2) + \rho_{k+1,0}\tilde{\rho}_{k+1,(0,L-1)} - \rho_{k,0}\tilde{\rho}_{k,(0,L-1)} \end{bmatrix} \quad (20)$$

$$\mathbf{G}(\mathbf{pR}_k - \mathbf{pR}_{k+2}) = \mathbf{H}_k - \mathbf{H}_{k+2} = \begin{bmatrix} \frac{1}{2} (\tilde{\rho}_{k+2,(0,1)}^2 - \tilde{\rho}_{k,(0,1)}^2) + \rho_{k+2,0}\tilde{\rho}_{k+2,(0,1)} - \rho_{k,0}\tilde{\rho}_{k,(0,1)} \\ \vdots \\ \frac{1}{2} (\tilde{\rho}_{k+2,(0,L-1)}^2 - \tilde{\rho}_{k,(0,L-1)}^2) + \rho_{k+2,0}\tilde{\rho}_{k+2,(0,L-1)} - \rho_{k,0}\tilde{\rho}_{k,(0,L-1)} \end{bmatrix} \quad (21)$$

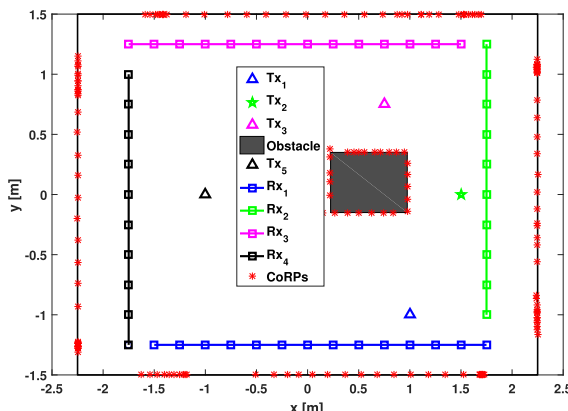


FIGURE 5. Indoor scenario for CoRP's Estimation using AoA with static transmitter and moving Receiver.

are biased due to noise, a clustering of all measurements is required. Without loss of generality, the K-means algorithm [33] has been used to cluster the set of estimates of the obstacle vertices. Then, the sum of absolute differences approach is implemented to specify the centroids of the clusters. The latter represent the component-wise median of a set of estimations for an obstacle vertex.

E. DISCUSSION ON MOSAIC

One AN was used so far for receiver localization and obstacle detection. If the obstacle is known then the estimation of the receiver position follows from the VANs positions. However, when the obstacle information is not available, the estimation of both the receiver and the VANs positions can be done if enough measurement metrics (TDoA and AoA, RSS and AoA) are available.

The estimation accuracy depends on the availability of LoS path. When it is not available, the measurements (mainly the AoA) will be biased since in our approach, the first path is considered to be the LoS. To overcome this problem and reduce the bias, it is very important to either use a tracking approach via for instance EKF or increase the number of ANs leading to an increase in the LoS measurements which implies a large number of points of reflection that could be used to determine the obstacle limits. On the other side, the limits of the obstacle are estimated if and only if the receiver is within the range of reflection. Nevertheless, this is not always the case with a single receiver at a given position and single AN as shown in Fig. 5. Consequently, tracking the obstacle limits via EKF or via a large number of ANs will also enhance the mapping accuracy. So, two questions arise: how do we include EKF in mapping? and how many ANs do we need in MOSAIC at a receiver position, i.e. without tracking?

V. TRACKING AND MAPPING VIA EKF

EKF, as all types of Kalman filter, consists of a hidden process that defines the updated state estimate and an observational process that defines the new measurements. The target of this section is to improve the obstacle detection and mapping via

EKF-based tracking. As the mapping in MOSAIC is mainly based on the estimation of the points of reflection at the obstacle side(s), the problem of tracking via EKF turns out to have a proper description of the CoRPs updates within EKF framework and its model. Again, in this section, we consider that the room is equipped with one Tx and one mobile Rx. With these hypothesis, the target now is to have a thorough description of the PoRs taking into account the estimation bias of the TDoA, AoA and RSS.⁵ This will be then followed by the description of the EKF framework in presence of the biased estimation.

A. POINTS OF REFLECTION IN PRESENCE OF METRIC ESTIMATION BIAS

Starting with (30), the estimated \mathbf{pS}_i in the presence of measurement noise (e.g. AoA error), can be written as follows:

$$\widehat{\mathbf{pS}}_i = \mathbf{pS}_i + \Delta \mathbf{pS}_i \quad (31)$$

where

$$\begin{aligned} \Delta \mathbf{pS}_i &= \Delta \mathbf{pR} + \text{inv}(\text{diag}(\mathbf{n}_i \cdot \mathbf{w}_i)) \\ &\cdot \left(\left(-\left(\frac{\Delta \mathbf{pR} - \Delta \mathbf{w}_i}{2} \right) \cdot \mathbf{n}_i - \Delta \mathbf{pV}_i \cdot \mathbf{q}_i \right) \mathbf{w}_i \right. \\ &\left. + (\mathbf{q}_i \cdot \mathbf{n}_i) \Delta \mathbf{w}_i \right) \end{aligned} \quad (32)$$

where \mathbf{q}_i , the vector passing through \mathbf{pR} and the midpoint between \mathbf{pT} and \mathbf{pV}_i ; \mathbf{n}_i , the normal to the point of reflection \mathbf{S}_i ; \mathbf{w}_i , the vector crossing the point of reflection \mathbf{pS}_i to the virtual receiver defined as the mirroring point of the receiver with respect to the obstacle, are defined as follows:

$$\mathbf{q}_i = \begin{bmatrix} \frac{xT + xV_i}{2} - xR \\ \frac{yT + yV_i}{2} - yR \end{bmatrix} \quad (33)$$

$$\mathbf{n}_i = \mathbf{pT} - \mathbf{pV}_i \quad (34)$$

$$\mathbf{w}_i = \mathbf{pV}_i - \mathbf{pR} \quad (35)$$

The errors of estimation $\Delta \mathbf{pR}$, $\Delta \mathbf{pV}_i$ and $\Delta \mathbf{w}_i$ for estimating \mathbf{pR} , \mathbf{pV}_i and \mathbf{w}_i are calculated based on the error on either the AoA measurements or TDoA measurements.

1) PoR ESTIMATION IN PRESENCE OF AoA BIAS

Assuming a biased estimation of the AoA, the error $\Delta \mathbf{pR}$ of estimating the receiver is given as follows :

$$\Delta \mathbf{pR} = \epsilon_\theta \cdot \rho_0 \begin{bmatrix} -\sin \theta_0 \\ \cos \theta_0 \end{bmatrix} \quad (36)$$

where ϵ_θ is the AoA error in radians. Hence, $\Delta \mathbf{pR}$ imposes an error $\Delta \mathbf{pV}_i$, the error of estimating the VAN \mathbf{pV}_i as:

$$\Delta \mathbf{pV}_i = \epsilon_\theta \left(\rho_0 \begin{bmatrix} -\sin \theta_0 \\ \cos \theta_0 \end{bmatrix} + \rho_i \begin{bmatrix} -\sin \theta_i \\ \cos \theta_i \end{bmatrix} \right) \quad (37)$$

⁵in this paper, we limit the description for the TDoA and AoA error only for the sake of homogeneity

Moreover, the error in AoA measurements impose an error of Δw_i for estimating w_i calculated as:

$$\Delta w_i = \epsilon_\theta \cdot \rho_i \begin{bmatrix} -\sin \theta_i \\ \cos \theta_i \end{bmatrix} \quad (38)$$

2) PoR ESTIMATION IN PRESENCE OF TDoA ERROR

On the other hand, assuming error in TDoA, ΔpR is given by:

$$\Delta pR = c \cdot \epsilon_t \cdot \begin{bmatrix} \sin \theta_0 \\ \cos \theta_0 \end{bmatrix} \quad (39)$$

where c is the speed of light, ϵ_t is the TDoA error in radians. Similarly, ΔpR imposes an error ΔpV_i that is:

$$\Delta pV_i = c \cdot \epsilon_t \cdot \left(\begin{bmatrix} \sin \theta_0 \\ \cos \theta_0 \end{bmatrix} + \begin{bmatrix} \sin \theta_i \\ \cos \theta_i \end{bmatrix} \right) \quad (40)$$

Finally, the error in TDoA measurements impose an error of Δw_i for estimating w_i calculated as:

$$\Delta w_i = c \cdot \epsilon_t \cdot \begin{bmatrix} \sin \theta_i \\ \cos \theta_i \end{bmatrix} \quad (41)$$

B. EKF MODEL IN TRACKING THE PoRs

In the previous subsection, we have provided the error model of the PoR depending on the biased measurements of the AoA and TDoA. The target is then to include these derivations in the EKF filter formulation. The latter allows a tracking of the PoR when the receiver is moving and provides an estimation of the obstacle limits by simply creating the CoRP. In contradiction with the previous section in which the PoRs are simply estimated, the EKF offers a smoothing of the obstacle sides hence, a better description and mapping of the environment. Saying that, the two processes of the EKF filter for the PoRs are provided as follows:

$$\begin{aligned} pR_k &= f(pR_{k-1}) + pQ_{k-1} \\ pS_{k,i} &= h(pR_k) + pZ_{k,i} \end{aligned} \quad (42)$$

The hidden and the observational processes for the PoR, f and h respectively, are defined as follows:

$$\begin{aligned} f &= \begin{bmatrix} xR_k \\ yR_k \end{bmatrix} \\ h &= \begin{bmatrix} xR_k \\ yR_k \end{bmatrix} + \text{inv}(\text{diag}(\mathbf{n}_i \cdot \mathbf{w}_i)) \cdot (\mathbf{q}_i \cdot \mathbf{n}_i) \end{aligned} \quad (43)$$

Thus, the standard deviation for the errors of the hidden and observational processes, pQ and pZ respectively, are easily deduced from (36) through (41) for each approach (i.e. TDoA and AoA). Then, the EKF is executed over a fixed number of realizations in order to settle down, and we record the innovation error obtained during each of these realizations.

VI. OPTIMAL NUMBER OF ANS

The target in this section is to explore the effect of increasing the number of ANs in terms of localization accuracy and mapping capabilities. Indeed, it has been shown in the previous section that the environment mapping depends on the

estimation of the VANs which depends on the localization accuracy of the receiver. However, increasing the number of ANs indefinitely leads to additional measurements to be processed from one side and might not provide the best accuracy from the other side. To answer this question, we derive the CRLB of each algorithm proposed in Section 4 at each position of the Rx.

A. CRLB DERIVATIONS WITH N ANS

The optimal number of ANs needed is analyzed via CRLB optimization for each metric.

1) CRLB FOR ALGORITHM 1 (THE TL APPROACH)

Here, we assume that the AoA measurements taken at the receiver coming from all ANs are independent. Assuming a wideband multipath model, we estimate the receiver position using the TL technique based on a Gaussian AoA model. This model represents scenarios where there is a strong LoS component that could be resolved by the receiver separately from multiple NLoS components due to local scattering. For a single transmitter pT with an AoA $\theta(pT)$ at the receiver, we consider a Gaussian LoS model with local scattering defined as:

$$p_{LOS}(\hat{\theta}/pT) = \frac{1}{\sqrt{2\pi}\sigma(1-2Q(\frac{\pi}{2\sigma}))} \exp\left(-\frac{(\hat{\theta}-\theta(pT))^2}{2\sigma^2}\right) \quad (44)$$

where $\hat{\theta} \in [0, \pi]$, $Q(t) = \int_t^\infty \exp(-t^2/2)/\sqrt{2\pi} dt$ and σ^2 is the estimation error variance, representing the spatial extent of scattering. Additionally, the remaining AoA measurements due to reflected and scattered NLoS paths are assumed to be virtually in LoS with VANs. Hence, the distribution of these NLoS paths is defined as follows:

$$\begin{aligned} p_{NLoS}(\hat{\theta}_i/pV_i) &= \frac{1}{\sqrt{2\pi}\sigma(1-2Q(\frac{\pi}{2\sigma}))} \\ &\times \exp\left(-\frac{(\hat{\theta}_i-\theta_i(pV_i))^2}{2\sigma^2}\right) \end{aligned} \quad (45)$$

where $\theta_i(pV_i)$ is the true AoA coming from the VAN pV_i to the receiver knowing that $pV_0 = pT$. Hence, the AoA estimates are generated for a wideband multipath model based on the following distribution:

$$\begin{aligned} p_{wideband}(\hat{\theta}_0, \hat{\theta}_1, \dots, \hat{\theta}_{L-1}/pT) \\ = p_{LOS}(\hat{\theta}_0/pT) p_{NLoS}(\hat{\theta}_1/pV_1) \dots p_{NLoS}(\hat{\theta}_{L-1}/pV_{L-1}) \end{aligned} \quad (46)$$

where L is the number of RRCs. Accordingly, the log-likelihood function for the estimates of the AoA for all RRCs is as follows:

$$L(\hat{\theta}_0, \hat{\theta}_1, \dots, \hat{\theta}_{L-1}/pT, pV) = -\sum_{i=0}^{L-1} \frac{(\hat{\theta}_i - \theta_i(pV_i))^2}{\sigma^2} \quad (47)$$

Based on what has been derived for single transmitter in terms of the probability density function (pdf) of the wideband multipath model in (46), the log-likelihood function for the estimates of the AoA for all RRCs corresponding to multiple transmitters (i.e. ANs) is as follows:

$$L\left(\hat{\theta}_1, \hat{\theta}_2, \dots, \hat{\theta}_{L-1} / \mathbf{pT}, \mathbf{pV}\right) = -\sum_{m=1}^M \sum_{i=1}^{L-1} \frac{\left(\hat{\theta}_i - \theta_i(\mathbf{pV}_{m,i})\right)^2}{\sigma^2} \quad (48)$$

where $\theta_i(\mathbf{pV}_{m,i})$ is the true AoA coming from the VAN $\mathbf{pV}_{m,i}$ corresponding to the transmitter \mathbf{pT}_m reaching the receiver \mathbf{pR} and $\mathbf{pV}_{m,0} = \mathbf{pT}_m$. Then, we construct the Fisher information matrix (FIM) $\mathbf{F}(\{\mathbf{pT}, V\})$ in order to calculate the CRLB, which is $\mathbf{F}^{-1}(\{\mathbf{pT}, \mathbf{pV}\})$. For the Gaussian model in (46), $\mathbf{F}(\{\mathbf{pT}, V\})$ is defined as follows (49), as shown at the bottom of the next page: where $\rho_{m,i}$ is the distance between $\mathbf{pV}_{m,i}$ corresponding to the transmitter \mathbf{pT}_m and the receiver \mathbf{pR} . Knowing that the total error of localizing the receiver is the sum of variances along x and y , we define the CRLB for localization under NLoS environment using the TL technique as follows:

$$\begin{aligned} CRLB_{\theta|NLoS} &= Tr\left(\mathbf{F}^{-1}(\{\mathbf{pT}, V\})\right) \\ &= \frac{\sigma^2 \sum_{m=1}^M \sum_{i=1}^{L-1} \frac{1}{\rho_{m,i}^2}}{\sum_{m=1}^M \sum_{i=1}^{L-1} \sum_{k=1, k \neq i}^{L-1} \frac{\sin^2(\theta_i - \theta_k)}{\rho_{m,i}^2 \rho_{m,k}^2}} \end{aligned} \quad (50)$$

In case of LoS environment, the CRLB for localization using TL technique based on AoA approach is as follows:

$$CRLB_{\theta|LoS} = \frac{\sigma^2 \sum_{m=1}^M \frac{1}{\rho_{m,LoS}^2}}{\sum_{m=1}^M \sum_{k=1, k \neq m}^{L-1} \frac{\sin^2(\theta_m - \theta_k)}{\rho_{m,LoS}^2 \rho_{k,LoS}^2}} \quad (51)$$

2) CRLB FOR ALGORITHM 2 (TDoA METRIC)

The TDoA measurements taken at the receiver from multiple ANs are assumed to be independent. The distances between the receiver and the VAN $\mathbf{pV}_{m,i}$ corresponding to the transmitter \mathbf{p}_m in absence of noise is represented as follows:

$$\begin{aligned} \rho_{m,(i,0)} &= c \cdot t_{m,(i,0)} = \rho_{m,i} - \rho_{m,0}, \\ m &= 1, \dots, M \& i = 1, \dots, L-1 \end{aligned} \quad (52)$$

where $t_{m,i}$ is the TDoA of the received signal at the pair of the VAN $\mathbf{pV}_{m,i}$ and the transmitter \mathbf{pT}_m respectively, and c is the speed of light. As shown in (52), the estimated TDoAs are converted to RDoA measurements creating a set of nonlinear equations describing the hyperbolic range difference. In realistic scenarios, RDoA measurements $\tilde{\rho}_{m,0}$ are obtained with noise and modeled as:

$$\begin{aligned} \tilde{\rho}_{m,(i,0)} &= \rho_{m,(i,0)} + \epsilon_{m,(i,0)} = \rho_{m,i} - \rho_{m,0} + \epsilon_{m,(i,0)}, \\ m &= 1, \dots, M \end{aligned} \quad (53)$$

where $i = 1, \dots, L-1$ and $\epsilon_{m,(i,0)}$ is the zero mean Gaussian random noise vector of the RDoA measurement with

a $(L-1) \cdot (L-1)$ covariance matrix Σ_d . Thus, the pdf of $\tilde{\rho}_{m,(i,0)}$ defined in (53) is as follows:

$$\begin{aligned} Pr(\tilde{\rho}; \rho) &= \prod_{m=1}^M \prod_{i=1}^{L-1} \frac{1}{\sqrt{2\pi c^2 \sigma_T^2}} \exp\left[-\frac{(\tilde{\rho}_{m,(i,0)} - \rho_{m,(i,0)})^2}{2c^2 \sigma_T^2}\right] \\ &= \frac{1}{(2\pi c^2 \sigma_T^2)^{\frac{M \cdot (L-1)}{2}}} \\ &\times \exp\left[-\frac{\sum_{m=1}^M \sum_{i=1}^{L-1} (\tilde{\rho}_{m,(i,0)} - \rho_{m,(i,0)})^2}{2c^2 \sigma_T^2}\right] \end{aligned} \quad (54)$$

Using the second partial derivative of the LLF for the pdf defined in (54), we obtain:

$$\frac{\partial^2 (\log(Pr(\tilde{\rho}; \rho)))}{\partial \rho^2} = -\frac{M \cdot (L-1)}{c^2 \sigma_T^2} \quad (55)$$

Consequently, the optimal number of ANs required to achieve a TDoA localization accuracy defined by the CRLB is as follows:

$$M_{optimal} = \frac{c^2 \sigma_T^2}{(L-1) \cdot CRLB_t} \quad (56)$$

3) CRLB FOR ALGORITHM 3 (RSS APPROACH)

See Appendix C

B. DISCUSSION

The CRLB of the different metrics decreases with the number of ANs, except for AoA, in which a further discussion should be provided. Indeed, when the AoA metric is used for localization and mapping, it is very important to separate between the LoS and NLoS cases. In the former, an additional number of ANs increases the resolvability of the Rx location as it will be shown in next section. However, in the case of NLoS, the increase in the ANs will increase the number of ambiguities hence it deteriorates the estimation. This is not the case in RSS or TDoA since they are used to support the TL approach. Another conclusion can be derived from the calculations of the CRLBs. Equations (73) and (56) show that the number M of ANs and the number L of RRCs can be exchanged without changing in the CRLB. This means that both RSS and TDoA present similar results if the number of anchor nodes is increased or the number of reflections is increased.

VII. SIMULATION RESULTS

A. PARAMETERS AND ENVIRONMENT SETTINGS

The room geometry is of rectangular shape of size $(10 \times 10)m^2$. The south-western corner of the room is assumed to be the reference of the Cartesian coordinate system. The angles are measured with respect to the positive part of the x-axis. The transmitter is set at position $\mathbf{pT} = (0.2, 0.2)$ m. The antenna at the transmitter is assumed to be omnidirectional; hence, the transmitted power $\mathbf{SP}(\theta)$ is constant for all θ . An antenna array is considered at the receiver

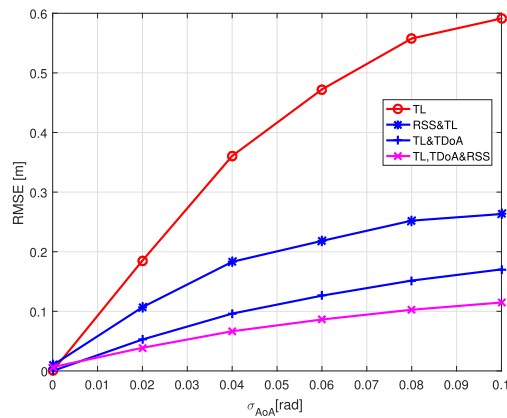


FIGURE 6. Simulation Results of the Hybrid Approach.

with a reception beam pattern described as $\mathbf{SP}(\theta) = \exp\left(-\frac{\theta^2}{2s^2}\right)$, $s = 0.1$. The value of parameter s and the Gaussian shape have been devised empirically. Additionally, all results are simulated for 10000 realizations.

B. PERFORMANCE OF THE RX LOCALIZATION ALGORITHM IN UNKNOWN ENVIRONMENT

In this section, we provide the simulation results of the localization accuracy in an unknown environment. We remind the reader that an unknown environment refers to the case where there is no information about the obstacles in the room.

We implemented different combinations of the basic standalone positioning techniques (TL, RSS, and TDoA) to achieve additional enhancement in the localization accuracy. Fig. 6 shows the RMSE of estimating the receiver's position using TL, TL in combination with TDoA, TL in combination with RSS and TL in combination with RSS and TDoA. It is very clear that the hybrid approach presents the best results. Particularly, the combination of the TL and TDoA has a good accuracy and presents comparable results with those obtained with all metrics. In terms of localizing VANs, Fig. 7 shows that the estimation error can be greatly reduced, reaching few centimeters, if the number of Rx measurements is high enough. For instance, the error is shown to be less than 0.075 m at $\sigma_{\text{TDOA}} = 0.2 \text{ ns}$ and less than 0.04 m at $\sigma_{\text{TDOA}} = 0.1 \text{ ns}$ with 100 Rx positions. This means that a mobile receiver can perfectly estimate the positions of the VANs.

C. EKF-SLAM

In this section, we aim at evaluating the importance of the EKF in mapping. We do so by evaluating the estimated

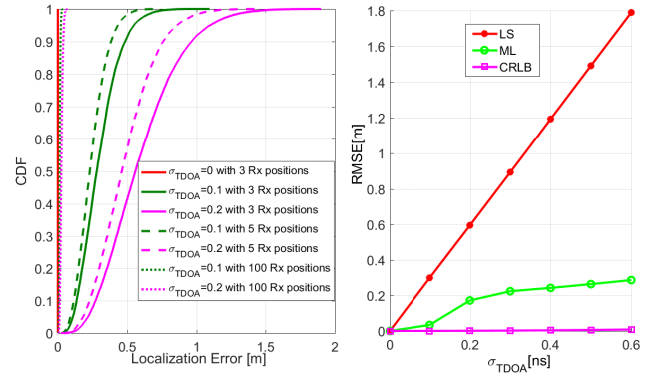
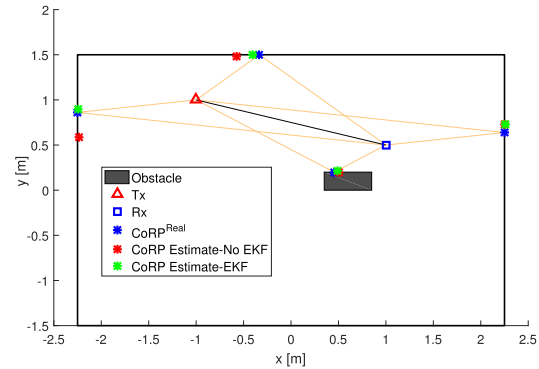
FIGURE 7. Estimation error of localizing VANs based on TDoA approach using LS and ML versus σ_{TDOA} .

FIGURE 8. Indoor scenario for CoRPs' Estimation.

PoRs. For simplicity purposes, the scenario shown in Fig. 8 is adopted. In this figure, the estimated PoR before and after EKF are shown. Moreover, Fig. 9 shows the RMSE for estimating the CoRP with and without EKF adopted in the previous sections for different values of the TDoA and AoA estimation bias.

D. OPTIMAL NUMBER OF ANS

Increasing the number of ANs is proposed for the sake of enhancing localization and obstacle mapping accuracy. This enhancement is expected to increase the probability of LoS links and the number of estimations for the obstacle vertices. Thus, the optimal number of ANs is recognized as a compromise between the number that achieves the best localization accuracy and the number that achieves full detection of an obstacle. As shown in Fig. 10, the localization accuracy for TL becomes worse with the growing number of ANs. The decrease of the CRLB level using TL as the number of ANs grows is due to the NLoS environment.

$$F(\{\mathbf{pT}, \mathbf{pV}\}) = \begin{pmatrix} \sum_{m=1}^M \sum_{i=1}^{L-1} \frac{\sin^2(\theta_i)}{\sigma^2 \rho_{m,i}^2} & - \sum_{m=1}^M \sum_{i=1}^{L-1} \frac{\cos(\theta_i) \sin(\theta_i)}{\sigma^2 \rho_{m,i}^2} \\ - \sum_{m=1}^M \sum_{i=1}^{L-1} \frac{\cos(\theta_i) \sin(\theta_i)}{\sigma^2 \rho_{m,i}^2} & \sum_{m=1}^M \sum_{i=1}^{L-1} \frac{\cos^2(\theta_i)}{\sigma^2 \rho_{m,i}^2} \end{pmatrix} \quad (49)$$

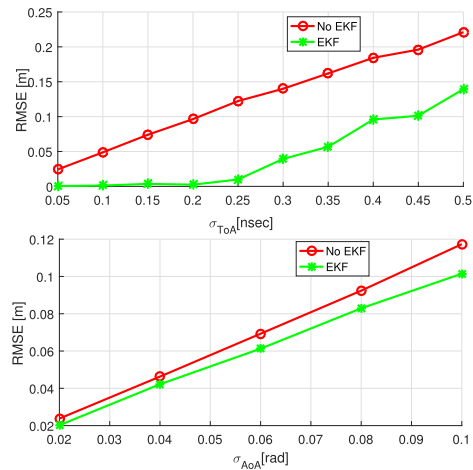


FIGURE 9. RMSE for estimating Point of Reflections versus σ_t and σ_θ .

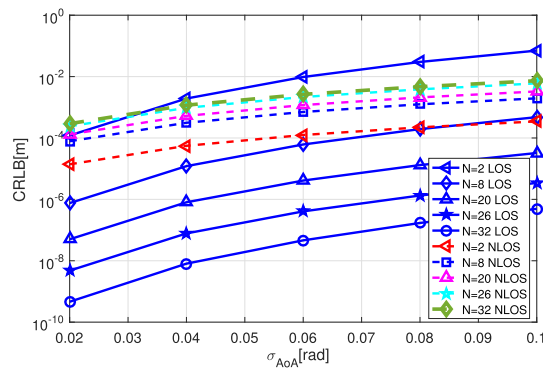


FIGURE 10. CRLB of localization accuracy using AoA under LoS/NLoS conditions for various number of ANs.

The AoA localization based technique is highly sensitive to errors under NLoS scenario since the rays coming from NLoS paths will deteriorate the localization accuracy. This is indeed expected as AoA is very sensitive to errors as shown in literature. For instance, an error of 5° might lead to high direction error which is translated by high position error.

However, in LoS conditions, higher number of ANs decreases the CRLB level of the localization accuracy as shown in Fig. 10. In such scenario, the AoA of the LoS ray is less biased to error compared to that of the NLoS ray; hence, the localization accuracy is enhanced with higher number of ANs. Moreover, the increase in the number of ANs is shown in Fig. 11 to decrease the CRLB using RSS and TDoA. Finally, as expected, the rise in the number of ANs is shown to enhance the mapping ability. It is very clear that at least 30 ANs are needed to have a good estimation of the VANs hence the obstacle vertices.

E. OBSTACLE MAPPING

After localizing the VANs, the obstacles in the room are to be mapped in terms of their positions, dimensions and limits. Three types of obstacles have been considered: a square,

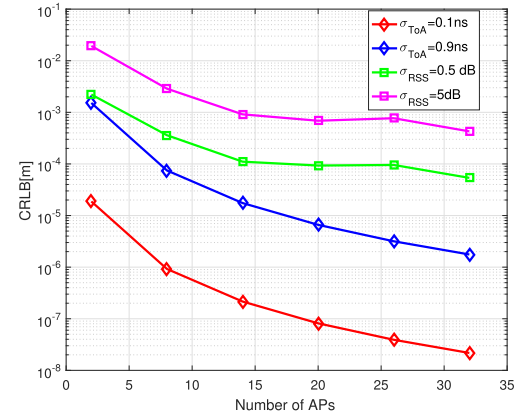


FIGURE 11. CRLB of localization accuracy versus number of ANs using TDoA and RSS.

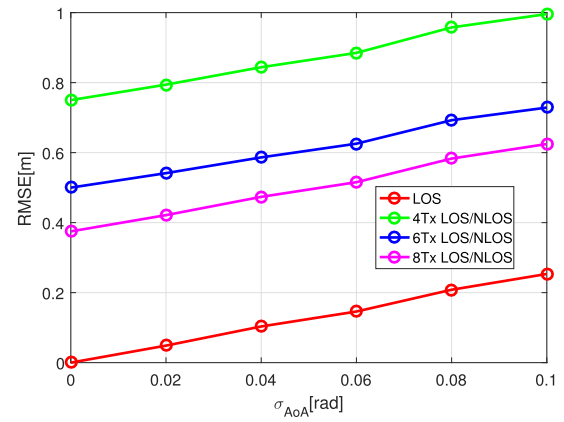


FIGURE 12. RMSE versus σ_{AoA} for estimating receiver under LoS/NLoS channel.

a triangle and a hexagon. Fig. 13 shows the estimated vertices of a triangular obstacle in the room with $M = 12$ and $M = 42$ ANs, respectively, using the TL (ref. Section IV.A) with $\sigma_{\text{AoA}} = 0.09 \text{ rad}$ (*almost* 5°) and the K-means algorithm to cluster the set of estimated obstacle vertices. It is very clear that the TL approach presents very good accuracy if the number of ANs is large enough. Moreover, the results are in line with CRLB derived in the previous section which specifies at least 30 ANs for good accuracy. Fig. 14 presents the mapping results of a square and hexagonal obstacles using TDoA approaches, provided in Section IV with $\sigma_{\text{TDoA}} = 0.05 \text{ ns}$ and $\sigma_{\text{TDoA}} = 0.1 \text{ ns}$, respectively. Here, the cloud of vertices points at each measurement is shown as well as the resulting estimated vertices using K-means algorithm.

F. APPLICATION TO REAL INDOOR ENVIRONMENT

MOSAIC was also implemented in indoor real environment thanks to the support of Siradel through their commercial 5G Channel Simulator [35]. As shown in Fig. 15, the colored scale shows the power variation of received rays. In this scheme, the rays with RSS higher than a threshold are kept and shown in right top corner in Fig. 15; they are used for

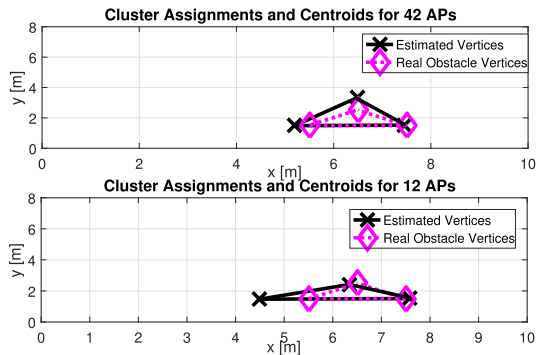


FIGURE 13. Obstacle (triangle) mapping using the TL approach to estimate the VANs.

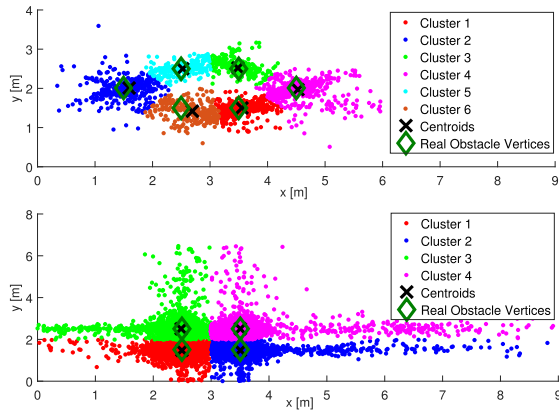


FIGURE 14. Obstacle (hexagon and Square) mapping using TDoA.

estimating the Rx and the CoRP. The RMSE of this scenario is shown in Fig. 16. It is very clear that an AoA bias up to few degrees provides a good estimation of the CoRP as well as the distances between the different points.

G. ANALYSIS AND CONCLUSIONS ON THE SIMULATIONS RESULTS

As shown in Fig. 12, the CRLB level of the TL (AoA-based approach) decreases with the growing number of ANs under LoS environment. Nevertheless, this is not the case with NLoS environment. However, as the obstacle mapping highly depends on the localization accuracy from one side and needs the reflection paths from the other side, it becomes very important to select the optimal number of ANs which is able to realize both localization and mapping. Another important point resides in the AoA measurement errors as they highly affect the accuracy of the obstacle mapping. However, thanks to the large number of antennas implemented in mmWave technology, these errors are very small [30]. Similarly, TDoA is shown to achieve high accuracy in terms of localizing VANs with respect to the noise variance of the TDoA measurements. In practice, the TDoA based approach provides a negligible estimation error in the localization approach. However, the mapping needs an

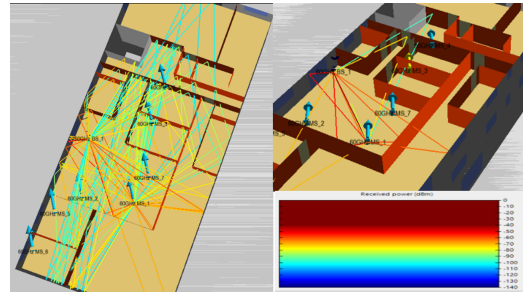


FIGURE 15. real indoor environment from 5G Channel Simulator.

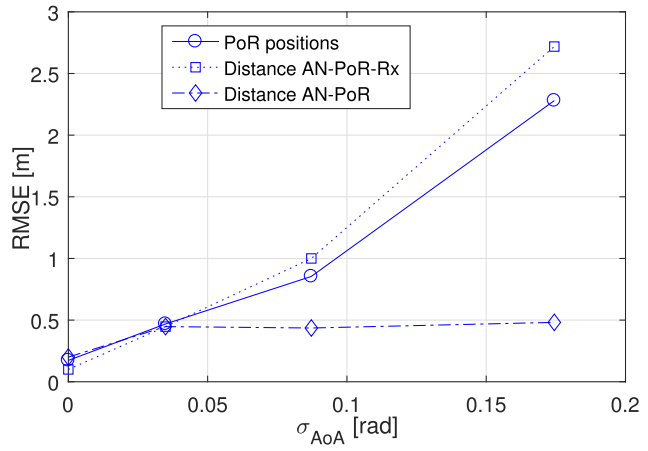


FIGURE 16. RMSE for the CoRP, Distance AN-PoR-Rx, Distance AN-PoR, Indoor Environment.

estimation of the AoA which again needs to be very accurate. In terms of raw accuracy, 10 GHz bandwidth is required to achieve accurate estimation using TDoA with an error in the order of 0.1 ns in terms of σ_t . This is indeed one advantage of using mmWave whose band can reach few GHz.

RSS based approach is the worst in terms of estimating the VANs positions due to an increased error in the Rx localization as shown in the CRLB given in Fig. 12. Moreover, this bias is increased in practice due to the absorption loss by the obstacles on the NLoS rays powers. Finally, it is worth mentioning that the simulation results have shown that the localization and mapping within the MOSAIC framework present an excellent accuracy reaching few centimeters if appropriate algorithms and parameters are selected.

VIII. CONCLUSION

In this paper, we presented MOSAIC a framework for joint localization and mapping. The concept is based on few steps based on localization of the receiver, followed by the estimation of the VANs and then obstacle mapping and dimensioning.

The performance of the localization techniques is tested through simulations in terms of RMSE and CDF of the location estimation error. In terms of obstacle detection, the paper proposed a new approach based on VANs and mirroring. A thorough analysis of the proposed approaches has been

made in the paper from theoretical and algorithmic point of view. EKF filter model has been adopted to improve the obstacle mapping accuracy reaching sub-cm.

Simulations have shown that finding the optimal number of ANs using the CRLB is a compromise between localization and obstacle mapping accuracy.

The paper consists a first of its kind in mapping an indoor environment based on the channel measurements. Definitely, much work could be achieved in the future. Among others, the localization and detection of multiple objects is a possible future direction. Also, the localization, detection and classification (object, human, etc) of moving objects will be of order in the future research directions.

APPENDIX A

ALGORITHM 3- RSS FOR ESTIMATING VANs

The RSS approach can be also used to estimate the positions of VANs required for obstacle detection. The received power at these anchor nodes follows a log-normal shadowing pathloss model in mmwave channels [31], [32]. The received power, P_i , is calculated using the following equation:

$$P_i [dBm] = P_0 - 10\eta \log_{10} \rho_i + \epsilon_i, i = 1, \dots, L-1 \quad (57)$$

where P_0 is the power at the reference distance ρ_0 , η is the pathloss exponent (PLE), ρ_i is the Euclidean distance between Rx and the VAN \mathbf{pV}_i , and ϵ_i is the zero mean Gaussian random variable measured in dB scale with shadowing fading effect described by the standard deviation σ_ρ . The square of the distance ρ_i between the VAN \mathbf{pV}_i and the receiver \mathbf{pR} is represented as follows:

$$\rho_i^2 = \|\mathbf{pV}_i - \mathbf{pR}\|_2^2 = (xV_i - xR)^2 + (yV_i - yR)^2 \quad (58)$$

Without loss of generality, we assume the transmitter to be the reference. Hence, for $i \geq 1$, we define the following:

$$xR \cdot \rho_i^2 - \rho_0^2 = xV_i^2 - 2xR \cdot xV_i + yV_i^2 - 2yR \cdot yV_i \quad (59)$$

Expressing (59) in matrix form, we obtain the following equation:

$$\begin{bmatrix} 2xV_1 & 2yV_1 \\ \vdots & \vdots \\ 2xV_{L-1} & 2yV_{L-1} \end{bmatrix} \cdot \begin{bmatrix} xR \\ yR \end{bmatrix} = \begin{bmatrix} xV_1^2 - xT^2 + yV_1^2 - yT^2 + \rho_0^2 - \rho_1^2 \\ \vdots \\ xV_{L-1}^2 - xT^2 + yV_{L-1}^2 - yT^2 + \rho_0^2 - \rho_{L-1}^2 \end{bmatrix} \quad (60)$$

The real distance ρ_i is not known in RSS localization; hence, noisy estimations of the distance, $\tilde{\rho}_i$, obtained from (57), are related with the unknown position of the receiver $\mathbf{pR} = [xR, yR]^T$ as follows:

$$\mathbf{R} \cdot \mathbf{pR} = \mathbf{T} \quad (61)$$

where \mathbf{R} and \mathbf{T} are defined as follows:

$$\mathbf{R} = \begin{bmatrix} 2(xV_1 - xT) & 2(yV_1 - yT) \\ \vdots & \vdots \\ 2(xV_{L-1} - xT) & 2(yV_{L-1} - yT) \end{bmatrix}$$

$$\mathbf{T} = \begin{bmatrix} xV_1^2 - xT^2 + yV_1^2 - yT^2 + \rho_0^2 - \rho_1^2 \\ \vdots \\ xV_{L-1}^2 - xT^2 + yV_{L-1}^2 - yT^2 + \rho_0^2 - \rho_{L-1}^2 \end{bmatrix}$$

Equation (61) can be extended to N different positions $\{\mathbf{pR}_k, \mathbf{pR}_{k+1}, \dots, \mathbf{pR}_N\}$. Hence, the following system of equations is generated based on the difference between the measurements taken at \mathbf{pR}_k and \mathbf{pR}_n , $n = k+1, \dots, k+N$, respectively:

$$\begin{aligned} \mathbf{R}(\mathbf{pR}_k - \mathbf{pR}_n) &= \mathbf{T}_1 - \mathbf{T}_n \\ &= \begin{bmatrix} \tilde{\rho}_{k,0}^2 - \tilde{\rho}_{k,1}^2 - \tilde{\rho}_{n,0}^2 + \tilde{\rho}_{n,1}^2 \\ \vdots \\ \tilde{\rho}_{k,0}^2 - \tilde{\rho}_{k,L-1}^2 - \tilde{\rho}_{n,0}^2 + \tilde{\rho}_{n,L-1}^2 \end{bmatrix} \end{aligned} \quad (62)$$

where $\tilde{\rho}_{n,i}^2$ is the estimated distance between VAN \mathbf{pV}_i and the receiver at position \mathbf{pR}_n , knowing that $\rho_{n,i}^2$ is defined as follows:

$$\rho_{n,i}^2 = \|\mathbf{pV}_i - \mathbf{pR}_n\|_2^2 = (xV_i - xR_n)^2 + (yV_i - yR_n)^2 \quad (63)$$

The target is to estimate \mathbf{R} in order to estimate the positions of the VANs. A simple Least Square (LS) estimator gives:

$$\hat{\mathbf{R}} = \mathbf{T}_d \cdot \mathbf{P}_d^T \left(\mathbf{P}_d \mathbf{P}_d^T \right)^{-1} \quad (64)$$

where \mathbf{T}_d and \mathbf{P}_d are now defined as follows:

$$\mathbf{P}_d = [\mathbf{pR}_k - \mathbf{pR}_{k+1} \quad \mathbf{pR}_k - \mathbf{pR}_{k+2} \quad \dots \quad \mathbf{pR}_k - \mathbf{pR}_N] \quad (65)$$

$$\mathbf{T}_d = [\mathbf{T}_1 - \mathbf{T}_2 \quad \mathbf{T}_1 - \mathbf{T}_3 \quad \dots \quad \mathbf{T}_1 - \mathbf{T}_N] \quad (66)$$

As a result, the positions of the VANs are estimated as follows:

$$\begin{bmatrix} xV_1 & yV_1 \\ \vdots & \vdots \\ xV_{L-1} & yV_{L-1} \end{bmatrix} = \frac{1}{2} \hat{\mathbf{R}} + \begin{bmatrix} xT & yT \\ \vdots & \vdots \\ xT & yT \end{bmatrix} \quad (67)$$

APPENDIX B

RSS-WLS SOLUTION

The aim here is to enhance the estimation taking into account the noise variance. We start with an example of 3 measurements and then the equations are updated accordingly. Equation (62) can be written as:

$$\mathbf{P}_{WLS} \cdot \mathbf{R}_{WLS} = \mathbf{T}_{WLS} \quad (68)$$

where \mathbf{P}_{WLS} , \mathbf{R}_{WLS} and \mathbf{T}_{WLS} are defined as follows:

$$\mathbf{P}_{WLS} = \begin{bmatrix} \mathbf{P}_{12}(1) & \mathbf{P}_{13}(1) & 0 & \dots & 0 \\ \mathbf{P}_{12}(2) & \mathbf{P}_{13}(2) & \dots & \ddots & \vdots \\ 0 & \dots & \ddots & \dots & \vdots \\ \vdots & \dots & \dots & \mathbf{P}_{12}(1) & \mathbf{P}_{13}(1) \\ 0 & \dots & \dots & \mathbf{P}_{12}(2) & \mathbf{P}_{13}(2) \end{bmatrix}$$

$$\mathbf{R}_{WLS} = \begin{bmatrix} 2(xV_2 - xV_1) \\ 2(yV_2 - yV_1) \\ \vdots \\ 2(xV_L - xV_1) \\ 2(yV_L - yV_1) \end{bmatrix}$$

$$\mathbf{T}_{WLS} = \begin{bmatrix} \mathbf{T}_d(1, 1) \\ \mathbf{T}_d(1, 2) \\ \vdots \\ \mathbf{T}_d(L-1, 1) \\ \mathbf{T}_d(L-1, 2) \end{bmatrix}$$

where $\mathbf{P}_{12} = \mathbf{pR}_k - \mathbf{pR}_{k+1}$ and $\mathbf{P}_{13} = \mathbf{pR}_k - \mathbf{pR}_{k+2}$. Additionally, knowing that the dimensions of \mathbf{R}_{WLS} and \mathbf{T}_{WLS} are $2 \cdot (L-1) \times 1$ and the dimension of \mathbf{P}_{WLS} is $2 \cdot (L-1) \times 2 \cdot (L-1)$. Hence, \mathbf{P}_{WLS} can be written as follows:

$$\mathbf{P}_{WLS} = \mathbf{I} \otimes \begin{bmatrix} \mathbf{P}_{12}(1) & \mathbf{P}_{13}(1) \\ \mathbf{P}_{12}(2) & \mathbf{P}_{13}(2) \end{bmatrix} \quad (69)$$

where \mathbf{I} is the identity matrix of dimension $(L-1) \times (L-1)$. Consequently, \mathbf{R}_{WLS} of the VANs can be estimated by:

$$\hat{\mathbf{R}}_{WLS} = \frac{1}{2} (\mathbf{W}_{WLS} \cdot \mathbf{P}_{WLS})^{-1} \mathbf{W}_{WLS} \cdot \mathbf{T}_{WLS} \quad (70)$$

where the weighting matrix \mathbf{W}_{WLS} is equal to the inverse of the covariance matrix Σ_{WLS} of the vector \mathbf{T}_{WLS} .

APPENDIX C CRLB FOR ALGORITHM 3 (RSS METRIC)

In RSS based approach, the log likelihood function (LLF) of the pdf of P_i is expressed as follows:

$$\log(Pr(\mathbf{PT}; \rho))$$

$$= \log \left(\prod_{m=1}^M \prod_{i=1}^{L-1} \frac{10/\log 10}{\sqrt{2\pi\sigma_\rho^2}} \frac{1}{P_{m,i}} \right.$$

$$\times \exp \left[-\frac{\left(\frac{10\eta}{\sigma_\rho \log 10}\right)^2}{8} \left(\log \frac{\rho_{m,i}^2}{\tilde{\rho}_{m,i}^2} \right)^2 \right] \left. \right)$$

$$= M \cdot (L-1) \cdot \log \left(\frac{10}{\log(10)\sqrt{2\pi\sigma_\rho^2}} \right)$$

$$+ \sum_{m=1}^M \sum_{i=1}^{L-1} \left(\log \left(\frac{1}{P_{m,i}} \right) - \frac{\left(\frac{10\eta}{\sigma_\rho \log 10}\right)^2}{2} \left(\log \left(\frac{\rho_{m,i}}{\tilde{\rho}_{m,i}} \right) \right)^2 \right) \quad (71)$$

where $\rho_{m,i}$ is the distance between the VAN $\mathbf{pV}_{m,i}$ corresponding to the transmitter \mathbf{pT}_m and the receiver \mathbf{pR} and $\tilde{\rho}_{m,i}$ is its estimate. Then, the second partial derivative is defined as follows:

$$\frac{\partial^2 (\log(Pr(\mathbf{P}; \rho)))}{\partial \rho^2}$$

$$= -\frac{\left(\frac{10\eta}{\sigma_\rho \log 10}\right)^2}{\ln 10} \sum_{m=1}^M \sum_{i=1}^{L-1} \frac{1}{\rho_{m,i}^2} \left(\frac{1}{\ln 10} - \log \left(\frac{\rho_{m,i}}{\tilde{\rho}_{m,i}} \right) \right) \quad (72)$$

Hence, the optimal number of ANs is obtained by optimizing the following CRLB for a target localization accuracy:

$$\text{CRLB}_{RSS} = \frac{-1}{\frac{\partial^2(\log(Pr(\mathbf{P}; \rho)))}{\partial \rho^2}}$$

$$= \frac{\ln 10}{\left(\frac{10\eta}{\sigma_\rho \log 10}\right)^2 \sum_{m=1}^M \sum_{i=1}^{L-1} \frac{1}{\rho_{m,i}^2} \left(\frac{1}{\ln 10} - \log \left(\frac{\rho_{m,i}}{\tilde{\rho}_{m,i}} \right) \right)} \quad (73)$$

REFERENCES

- [1] T. Rappaport *et al.*, *Millimeter Wave Wireless Communications*. London, U.K.: Pearson Education, 2014.
- [2] S. Rangan, T. S. Rappaport, and E. Erkip, “Millimeter-wave cellular wireless networks: Potentials and challenges,” *Proc. IEEE*, vol. 102, no. 3, pp. 366–385, Mar. 2014.
- [3] A. Küpper, *Location-Based Services*. Hoboken, NJ, USA: Wiley, 2005.
- [4] M. Bocquet *et al.*, “Comparison between 60-GHz UWB frequency modulation and UWB impulse-radio location systems,” in *Proc. Eur. Radar Conf. (EuRAD)*, Oct. 2008, pp. 41–43.
- [5] H. R. Fang, G. P. Cao, E. A. Ghara, K. Tom, and K. Mouthaan, “60 GHz short range planar RSS localization,” in *Proc. Asia-Pacific Microw. Conf.*, Dec. 2010, pp. 1396–1399.
- [6] A. Jafari, J. Sarrazin, D. Lautru, A. Benlarbi-Delai, L. Petrillo, and P. De Doncker, “NLOS influence on 60 GHz indoor localization based on a new TDOA extraction approach,” in *Proc. Eur. Microw. Conf.*, Nuremberg, Germany, Oct. 2013, pp. 330–333.
- [7] L. Subrt, P. Pechac, and S. Zvanovec, “New approach to modeling of diffuse reflection and scattering for millimeter-wave systems in indoor scenarios,” *PIERS Online*, vol. 6, no. 8, pp. 719–722, 2010.
- [8] N. Peinecke, H. Doebler, and B. Korn, “Phong-like lighting for MMW radar simulation,” in *Proc. SPIE*, vol. 7117, p. 71170M, Oct. 2008.
- [9] A. Maltsev, R. Maslennikov, A. Sevastyanov, A. Khoryaev, and A. Lomayev, “Experimental investigations of 60 GHz WLAN systems in office environment,” *IEEE J. Sel. Areas Commun.*, vol. 27, no. 8, pp. 1488–1499, Oct. 2009.
- [10] T. S. Rappaport *et al.*, “Millimeter wave mobile communications for 5G cellular: It will work!” *IEEE Access*, vol. 1, pp. 335–349, 2013.
- [11] G. R. MacCartney *et al.*, “Path loss models for 5G millimeter wave propagation channels in urban microcells,” in *Proc. IEEE GLOBECOM*, Atlanta, GA, USA, Dec. 2013.
- [12] T. S. Rappaport, F. Gutierrez, Jr., E. Ben-Dor, J. N. Murdock, Y. Qiao, and J. I. Tamir, “Broadband millimeter-wave propagation measurements and models using adaptive-beam antennas for outdoor urban cellular communications,” *IEEE Trans. Antennas Propag.*, vol. 61, no. 4, pp. 1850–1859, Apr. 2013.
- [13] M. W. M. G. Dissanayake, P. Newman, S. Clark, H. F. Durrant-Whyte, and M. Csorba, “A solution to the simultaneous localization and map building (SLAM) problem,” *IEEE Trans. Robot. Autom.*, vol. 17, no. 3, pp. 229–241, Jun. 2001.
- [14] W. Morris, I. Dryanovski, and J. Xiao, “3D indoor mapping for micro-uavs using hybrid range finders and multi-volume occupancy grids,” in *Proc. RSS 2010 Workshop RGB-D: Adv. Reasoning With Depth Cameras*, 2010, pp. 1–7.
- [15] H. Durrant-Whyte and T. Bailey, “Simultaneous localization and mapping: part I,” *IEEE Robot. Autom. Mag.*, vol. 13, no. 2, pp. 99–110, Jun. 2006.
- [16] A. Guerra, F. Guidi, and D. Dardari, “Position and orientation error bound for wideband massive antenna arrays,” in *Proc. IEEE Int. Conf. Commun.*, Jun. 2015, pp. 853–858.
- [17] W. Hong, K.-H. Baek, Y. Lee, Y. Kim, and S.-T. Ko, “Study and prototyping of practically large-scale mmWave antenna systems for 5G cellular devices,” *IEEE Commun. Mag.*, vol. 52, no. 9, pp. 63–69, Sep. 2014.
- [18] H. Kaouach, “Wideband low-loss linear and circular polarization transmitarrays in V-Band,” *IEEE Trans. Antennas Propag.*, vol. 59, no. 7, pp. 2513–2523, Jul. 2011.

- [19] J. Hoydis, S. ten Brink, and M. Debbah, "Massive MIMO in the UL/DL of cellular networks: How many antennas do we need?" *IEEE J. Sel. Areas Commun.*, vol. 31, no. 2, pp. 160–171, Feb. 2013.
- [20] E. G. Larsson, F. Tufvesson, O. Edfors, and T. L. Marzetta, (2013). "Massive MIMO for next generation wireless systems." [Online]. Available: <https://arxiv.org/abs/1304.6690v3>
- [21] F. Guidi, A. Guerra, and D. Dardari, "Millimeter-wave massive arrays for indoor SLAM," in *Proc. IEEE Int. Conf. Commun. Workshops (ICC)*, Sydney, NSW, Australia, Jun. 2014, pp. 114–120.
- [22] A. Guerra, F. Guidi, and D. Dardari, "Millimeter-wave personal radars for 3D environment mapping," in *Proc. IEEE Asilomar Conf. Signals, Syst. Comput.*, Pacific Grove, CA, USA, Nov. 2014, pp. 701–705.
- [23] C. Wu, Z. Yang, and Y. Liu, "Smartphones based crowdsourcing for indoor localization," *IEEE Trans. Mobile Comput.*, vol. 14, no. 2, pp. 444–457, Feb. 2015.
- [24] A. Guerra, F. Guidi, A. Clemente, R. D'Errico, L. Dussopt, and D. Dardari, "Application of transmitarray antennas for indoor mapping at millimeter-waves," in *Proc. IEEE Eur. Conf. Netw. Commun.*, Jun./Jul. 2015, pp. 77–81.
- [25] F. Guidi, A. Guerra, and D. Dardari, "Personal mobile radars with millimeter-wave massive arrays for indoor mapping," *IEEE Trans. Mobile Comput.*, vol. 15, no. 6, pp. 1471–1484, Jun. 2016.
- [26] C. Floerkemeier, M. Langheinrich, E. Fleisch, F. Mattern, and S. E. Sarma, Eds., *The Internet of Things: First International Conference*. Springer, 2008.
- [27] H. El-Sayed, G. Athanasiou, and C. Fischione, "Evaluation of localization methods in millimeter-wave wireless systems," in *Proc. IEEE 19th Int. Workshop Comput. Aided Modeling Design Commun. Links Netw. (CAMAD)*, Athens, Greece, Dec. 2014, pp. 345–349.
- [28] A. Olivier, G. Bielsa, I. Tejado, M. Zorzi, J. Widmer, and P. Casari, "Lightweight indoor localization for 60-GHz millimeter wave systems," in *Proc. 13th Annu. IEEE Int. Conf. Sens., Commun., Netw. (SECON)*, London, U.K., Jun. 2016, pp. 1–9.
- [29] A. Yassin, Y. Nasser, M. Awad, and A. Al-Dubai, "Simultaneous context inference and mapping using mm-Wave for indoor scenarios," in *Proc. IEEE Int. Conf. Commun. (ICC)*, Paris, France, May 2017, pp. 1–6.
- [30] A. Shahmansoori, G. E. Garcia, G. Destino, G. Seco-Granados, and H. Wymeersch, "Position and orientation estimation through millimeter-wave MIMO in 5G systems," *IEEE Trans. Wireless Commun.*, vol. 17, no. 3, pp. 1822–1835, Mar. 2018. [Online]. Available: <https://arxiv.org/abs/1702.01605>
- [31] T. Kos, M. Grgic, and G. Sisul, "Mobile user positioning in GSM/UMTS cellular networks," in *Proc. ELMAR*, Zadar, Croatia, Jun. 2006, pp. 185–188.
- [32] P. Meissner, T. Gigl, and K. Witrusal, "UWB sequential Monte Carlo positioning using virtual anchors," in *Proc. IPIN*, Zurich, Switzerland, Sep. 2010, pp. 1–10.
- [33] L. Cheng, X. Wu, and Y. Wang, "A non-line of sight localization method based on k-means clustering algorithm," in *Proc. 7th IEEE Int. Conf. Electron. Inf. Emergency Commun. (ICEIEC)*, Macau, China, Jul. 2017, pp. 465–468.
- [34] A. Yassin, Y. Nasser, and M. Awad, "Geometric approach in simultaneous context inference, localization and mapping using mm-wave," in *Proc. 25th Int. Conf. Telecommun. (ICT)*, Saint-Malo, France, Jun. 2018, pp. 1–6.
- [35] [Online]. Available: https://www.siradel.com/software/connectivity/s_5gchannel/



ALI YASSIN received the B.E. and M.E. degrees from the American University of Beirut, Lebanon, in 2012 and 2014, respectively, where he is currently pursuing the Ph.D. degree with the ECE Program. The major area of his Ph.D. degree is communication systems and the minor area is networking and security. Since 2014, he has been a Research Assistant with the American University of Beirut. His thesis on Context Inference, Localization and Mapping in Indoor Environments using mmWaves. His research interests are in intelligent localization and mapping techniques using millimeter waves in massive MIMO systems for indoor scenarios in addition to cooperative positioning and localization techniques in HetNet and cognitive network.



YOUSSEF NASSER (S'06–M'10–SM'11) received the master's and Ph.D. degrees in signal processing and communications from the National Polytechnic Institute of Grenoble, France, in 2003 and 2006, respectively, and the Habilitation à Diriger la Recherche degree, the highest education degree a scholar can achieve, in 2015.

From 2003 to 2006, he was with the Laboratory of Electronics and Information Technologies, Grenoble (Laboratoire d'Electronique et de Technologies de l'Information -LETI) as a Research and Development Engineer. From 2006 to 2010, he was a Senior Research Engineer with the Institute of Electronics and Telecommunications of Rennes, France. He is currently with the Department of Electrical and Computer Engineering, American University of Beirut.

He has published more than 100 papers in international peer-reviewed journals and conferences. Since 2007, he has been involved in the standardization of European broadcasting systems, including DVB-T2, DVB-T2 Lite, and DVB-NGH. He has coordinated tasks and/or packages of many European projects. These projects received the Golden and Silver awards from the European Union for their achievements. He is currently coordinating different projects on localization in heterogeneous networks, on convergence between DVB and LTE systems, and on 5G cellular system. He has served as a keynote speaker in different conferences, provided different tutorials in conferences and European institutions, and served as a guest editor-in-chief of many journals.



AHMED Y. AL-DUBAI (S'01–M'03–SM'08) received the B.Sc. degree in computer science from Mutah University in 1996, the M.Sc. degree in computer science from Al al-Bayt University in 1999, and the Ph.D. degree in computing from the University of Glasgow in 2005. He is currently a Professor with the School of Computing, where he leads the Networks Research Group, Edinburgh Napier University. His research interests span the areas of pervasive and mobile computing, communication protocols and algorithms, intelligent communication and networks, and Internet of Things. He led several projects funded by the Scottish Funding Council, EU, Carnegie Trust, Royal Society, World Bank, and other international funding bodies. He published widely in top-tier journals and leading IEEE/ACM international conferences. He is a member of several editorial boards of scholarly journals. He is a fellow of the British Higher Education Academy. He was a recipient of several international academic awards and recognitions, including best papers awards at several international ACM/IEEE conferences. Moreover, he served as the chair/co-chair of more than 30 international conferences and workshops. He is a guest editor for more than 20 special issues in international journals.



MARIETTE AWAD received the Ph.D. degree in electrical engineering in 2007. Prior to her academic position, she was with the IBM System and Technology Group, VT, USA, as a Wireless Product Engineer. She was invited by CVC labs, Google, and Qualcomm to present her work on machine learning and image processing. She has been a Visiting Professor with Virginia Commonwealth University, Intel Mobile Group, and MIT. She is currently an Associate Professor with the Engineering Department, American University of Beirut. She has published a book *Efficient Machine Learning* in 2015 and in numerous conferences and journals and is managing few grants. Her current research interests include machine learning, data analytics, and Internet of Things. She is a reviewer for the IEEE TRANSACTIONS. Over the years, her technical leadership and innovative spirit has earned her management recognition, several business awards, and multiple patents at IBM.